HHS Public Access

Author manuscript

BJU Int. Author manuscript; available in PMC 2016 January 15.

Published in final edited form as:

BJU Int. 2014 December ; 114(0): E105–E112. doi:10.1111/bju.12750.

Prostate tumour volumes: evaluation of the agreement between magnetic resonance imaging and histology using novel co-registration software

Julien Le Nobin[*,†], **Clément Orczyk**[*,‡], **Fang-Ming Deng**[§], **Jonathan Melamed**[§], **Henry Rusinek**[¶], **Samir S. Taneja**[*], and **Andrew B. Rosenkrantz**[¶]

[*]Department of Urology, Division of Urological Oncology, New York University Langone Medical Center, New York, NY, USA

[§]Department of Pathology, New York University Langone Medical Center, New York, NY, USA

[¶]Department of Radiology, New York University Langone Medical Center, New York, NY, USA

[†]Department of Urology, University Hospital of Lille, Lille

[‡]Department of Urology and Renal Transplantation/UMR 6301-Cervoxy Group, University Hospital of Caen, Caen, France

Abstract

Objective—To evaluate the agreement between prostate tumour volume determined using multiparametric magnetic resonance imaging (MRI) and that determined by histological assessment, using detailed software-assisted co-registration.

Materials and Methods—A total of 37 patients who underwent 3T multiparametric MRI (T2-weighted imaging [T2WI], diffusion-weighted imaging [DWI]/apparent diffusion coefficient [ADC], dynamic contrast-enhanced [DCE] imaging) were included. A radiologist traced the borders of suspicious lesions on T2WI and ADC and assigned a suspicion score of between 2 and 5, while a uropathologist traced the borders of tumours on histopathological photographs. Software was used to co-register MRI and three-dimensional digital reconstructions of radical prostatectomy specimens and to compute imaging and histopathological volumes. Agreement in volumes between MRI and histology was assessed using Bland–Altman plots and stratified by tumour characteristics.

Results—Among 50 tumours, the mean differences (95% limits of agreement) in MRI relative to histology were −32% (−128 to +65%) on T2WI and −47% (−143 to +49%) on ADC. For all tumour subsets, volume underestimation was more marked on ADC maps (mean difference ranging from −57 to −16%) than on T2WI (mean difference ranging from −45 to +2%). The 95% limits of agreement were wide for all comparisons, with the lower 95% limit ranging between −77

Correspondence: Julien Le Nobin, Department of Urology, Hôpital Claude Huriez, CHRU de Lille, 1, place de Verdin, 59037 Lille cedex, France. julien.lenobin@gmail.com.

Conflict of Interest

J.L.N, C.O., H.R., F.-M.D., J. M. and A.B.R. have nothing to disclose. S.S.T. is a consultant for GTX, Healthtronics and Bayer, speaker for Janssen, and has royalties from Elsevier, but has no direct financial conflict of interest.

and −143% across assessments. Volume underestimation was more marked for tumours with a Gleason score ≥7 or a MRI suspicion score 4 or 5.

Conclusion—Volume estimates of prostate cancer using MRI tended to substantially underestimate histopathological volumes, with a wide variability in extent of underestimation across cases. These findings have implications for efforts to use MRI to guide risk assessment.

Keywords

prostate cancer; diffusion-weighted MRI; histology; tumour volume; image processing; computer-assisted

Introduction

There is a growing range of options for the treatment of prostate cancer (PCa), including radical prostatectomy, radiation therapy, active surveillance and investigational focal ablative therapy. MRI provides the most widely used imaging test for depicting focal prostate lesions, and the ability to precisely define the volume of identified lesions using MRI would be of immense value for candidate selection, for guiding therapy and for monitoring both surveillance and treatment. A number of previous studies have suggested that MRI has limited value in predicting the volume of PCa [1-6], but the results of such studies may be difficult to apply to contemporary PCa management, given their use of older technology, lack of focus on index lesions and statistical methods that mainly explore volume correlations between imaging and histopathology [1-6]. While positive correlations may be useful for establishing the role of MRI in guiding prognosis and risk estimates, strong correlations do not guarantee a high level of consistency in predicting actual volumes, thereby limiting the impact of these results in risk assessment. While a more recent study did improve on earlier work by exploring the associations between volumes of PCa index lesions determined using multiparametric MRI at 3T and histopathology [7], that study also mainly used correlative statistics. Furthermore, histopathological tumour volumes in that study were determined using the ellipsoid formula, which is prone to error [8]. We have previously developed and validated a novel software tool that can determine the volume of three-dimensional (3D) digitally rebuilt histological specimens as well as perform accurate automated 3D deformable transformation and co-registration of such specimens with MRI [9]. This tool can correct for shrinkage and deformation of the prostate caused by the myriad of steps involved in the surgical procedure itself and by subsequent histological processing. The tool may be useful for more reliably estimating the performance of MRI in predicting actual tumour volumes and thereby determining the clinical impact of MRI in guiding candidate selection and treatment. The aim of the present study was to evaluate the level of agreement in volumes of PCa index lesions between histopathology and MRI, using novel co-registration software. We also assess the impact of various features, such as the MRI sequence and tumour grade, location and imaging appearance, on this level of agreement.

Materials and Methods

Study Population

This retrospective single-institution study was compliant with the Health Insurance Portability and Accountability Act and approved by our institutional review board with a waiver for informed consent. A total of 66 patients who underwent radical prostatectomy for PCa between November 2012 and July 2013 were identified. A number of patients were then excluded for the following reasons: they had not undergone preoperative MRI at our centre (n = 11); a full set of pathological images was unavailable (n = 11); no dominant tumour was identified on histological assessment (n = 2); an index lesion was not identified on preoperative MRI (n = 4); or there was no tumour on pathological examination (pT0 disease) [10] (n = 1). Patients with no visible tumour lesion on MRI were excluded because such patients would not be candidates MRI-guided focal lesion ablation. After these exclusions, the final cohort included 37 patients (mean age 60 ± 9 years) with a median (range) preoperative PSA 5.0 (0.32–98) ng/mL.

MRI Data Acquisition

All patients underwent multiparametric MRI using a 3T system (MAGNETOM Trio, Siemens Healthcare, Erlangen, Germany) and a pelvic phased-array coil. Examinations included non-enhanced multiplanar turbo spin-echo T2-weighted imaging (T2WI; slice thickness 3 mm, no interslice gap; field of view 180 × 180 mm; matrix 256 × 256), axial turbo spin-echo T1-weighted imaging (slice thickness 3 mm, no interslice gap; field of view 180 × 180 mm; matrix 192 × 192), axial diffusion-weighted imaging (DWI) (b-values between 50 and 1000 s/mm^2) with inline reconstruction of the apparent diffusion coefficient (ADC) map (slice thickness 3 mm, no interslice gap; field of view 200 × 200 mm; matrix 100 × 100), as well as dynamic contrast-enhanced (DCE) imaging of the prostate using 0.1 mmol/kg of gadolinium chelate (partition thickness 3 mm; field of view 240 × 240 mm; matrix 128 × 128). Contrast was injected using a power injector (Spectris; Medrad, Warrendale, PA, USA).

Histopathological Analysis

Prostatectomy specimens were processed according to standard institutional protocol. Specimens underwent fixation for 24 h after immediate fine-needle injection with formalin. The specimen was then cut at regular 5-mm intervals perpendicular to the posterior capsule, and intact slices were photographed using a digital camera at 210 pixels per cm and with a 1024 × 1366 matrix, thereby allowing appreciation of zonal anatomy on the photographs. Slices were then cut into quadrants, embedded in paraffin on 3–4-micron slides and stained with haematoxylin and eosin; four very large prostates were cut into sextants. The stained histology slides were digitalised in high resolution (400× magnification) using a Leica scanner SN 400 (Leica Microsystems, Wetzlar, Germany). These images were then rebuilt into a whole-mount image by border alignment and comparison with the previous photographs of the intact slices using Photoshop CS5 (Adobe Systems Inc, San Jose, CA, USA). A single uropathologist traced the border of all tumours on each slice and assigned a Gleason score based on the previously published consensus criteria. Lesions measuring <0.1 mL were excluded (n = 2).

MRI Assessment

A single genito-urinary radiologist was given a description of the approximate location of each tumour for each patient (left vs right, anterior vs posterior, base, middle or apex) but no other information regarding lesion size, location or grade. The radiologist then identified a corresponding abnormality in that region most likely to represent the tumour, based upon joint review of T2WI, DWI and DCE. This approach was used to simulate the clinical and investigational paradigms by which targeted biopsy and treatment are currently performed, directed to a lesion identifiable on MRI [11]. Then, the radiologist traced the margins of the lesion on each slice on which it was visible on both the axial T2WI and the ADC map. This radiologist also assigned a suspicion score to each lesion using a 1–5 Likert scale to indicate the probability of the lesion representing a significant cancer, generally based on previously published criteria [12]. These scores were then combined into a binary classification with scores 2–3 indicating low suspicion and scores 4–5 indicating high suspicion. Given that all included lesions were visible on MRI and that a score of 1 is used at our institution to indicate a negative MRI, all lesions received a suspicion score of at least 2. This binary division was based on previous work from our institution showing a substantial increase in cancer yield and grade among lesions with a score of 4 or 5, compared with lesions with a lower score [13].

Co-registration between MRI and Histopathology

Co-registration was performed using a previously validated method. Digital 3D representations of the surgical specimens were assembled using the digital photographs of the intact slices using computer software (ImageJ® and Photoshop; Adobe), providing 3D datasets for co-registration with MRI. This co-registration between MRI and the 3D digital gross specimens was performed using in-house software (FireVoxel); that uses both a manually directed landmark-based component and an automatic Mutual Information process. For the landmark-based component, the operator indicates a set of identical internal points of interest within each of the two image sets. For this purpose, corresponding landmarks relating to prostate zonal anatomy were selected on T2WI and the 3D rebuilt specimen. A combination of eight landmarks was extracted based on the zonal anatomy: distal urethra at the level of the apex; proximal urethra at the level of the base; verumontanum; anterior-most aspect of the anterolateral horn of the peripheral zone; anterior-most margin of the prostate; posterior junction of peripheral and transition zones; and left and right ejaculatory ducts. Co-registration was then performed to attain alignment of these landmarks within a mutually defined space, thus achieving co-registration of the whole image. The software allows the operator to analyse the consistency of each transformation by overlaying the source and target data and modifying each of these in real-time.

For each case, to first assess the accuracy of co-registration, the margins of the entire prostate were traced on axial T2WI and the 3D specimen, and the volume of the prostate on each of these image sets was determined after co-registration. Then, the ADC map was registered to the axial T2WI using the software's Mutual Information process. Subsequently, for each tumour, three regions of interest were generated: one representing the lesion defined on T2WI, one representing the lesion defined on ADC following co-registration to

T2WI, and one representing the lesion defined on 3D histology with co-registration to T2WI, which was referred to as the registered histology (ReH) lesion (Figs 1, 2). The software was then used to obtain the volume of each of these regions of interest for each tumour in the co-registered 3D space.

Statistical Analysis

Agreement between volumes determined using ReH and MRI was assessed using Bland–Altman analyses. This approach provides both the mean difference between the measurements (taking into account both the direction and magnitude of any difference) and the 95% limits of agreement (representing the mean difference ±1.96 SD of the difference, thereby indicating the expected range of variability between MRI and ReH measurements for the large majority of cases). The comparison was performed between volumes of the entire prostate determined on T2WI and 3D histology as well as between volumes of tumours determined on ReH and on T2WI and the ADC maps. Given a positive association between lesion volume and difference in volume between the techniques, the Bland–Altman analysis of tumour volumes was conducted in terms of percent differences. In addition, these assessments were performed for tumours stratified by various imaging and histological characteristics (Gleason score [6 vs ≥7], zone [peripheral vs transition] and MRI suspicion score [1–3 vs 4–5]). A *post hoc* analysis was performed comparing those lesions larger on T2WI than on ReH with the remaining lesions; these tumours were compared in terms of volume on ReH using the unpaired *t*-test and in terms of MRI suspicion score using the Mann–Whitney *U*-test. Statistical analysis was performed using MedCalc for Windows, version 12.7 (MedCalc Software, Ostend, Belgium).

Results

Comparison of Entire Prostate Volumes

The entire prostate in the 37 included patients had a mean volume on registered histopathology of 46.6 ± 16.3 mL and on T2WI of 46.9 ± 16.2 mL. The mean difference in prostate volumes between T2WI and registered histopathology was 0.37 mL, with 95% limits of agreement of −6.97 to +7.72 mL.

Lesion Characteristics

A total of 50 tumours were identified in the 37 prostatectomy specimens. Of these, 80.0% (40/50) were in the peripheral zone and 20.0% (10/50) were in the transition zone. The distribution of Gleason scores was as follows: 22.0% (11/50) Gleason 6; 76.0% (38/50) Gleason 7; 0% (0/50) Gleason 8; and 2.0% (1/50) Gleason 9. In all, 28.0% of tumours (14/50) had a low MRI suspicion score and 72.0% (36/50) had a high MRI suspicion score. The characteristics of patients and lesions are summarized in Table 1 and Fig 3.

Assessment of Lesion Volumes

The 50 tumours had a mean volume on ReH of 1.38 ± 1.20 mL, on T2WI of 0.93 ± 0.79 mL, and on ADC of 0.86 ± 0.78 mL. Table 2 summarizes the results of the Bland–Altman assessments. Overall, MRI substantially underestimated lesion volumes, and had wide 95%

limits of agreement. The mean difference and associated 95% limits of agreement on MRI relative to ReH were −32% (−128 to +65%) on T2WI and −47% (−143 to +49%) on ADC.

Table 2 also presents results for tumours stratified into various subsets. For all subsets, there was a more marked underestimation of volumes on the ADC maps (mean difference ranging from −57 to −16%) than on T2WI (mean difference ranging from −45 to +2%). Nonetheless, 95% limits of agreement were wide for all comparisons, with the lower 95% limit ranging between −77 and −143% across all assessments. There was more marked underestimation of volumes for tumours with Gleason score ≥7 or with an MRI suspicion score of 4 or 5. Transition zone tumours showed slightly more pronounced underestimation of lesion volumes on T2WI, although similar underestimation on ADC, compared with peripheral zone tumours. For both T2WI and ADC, the limits of agreement were slightly wider for smaller tumours. The extent of volume underestimation was somewhat less for smaller lesions on T2WI, although essentially identical between smaller and larger lesions for ADC.

A *post hoc* analysis of the 10 tumours larger on T2WI than on ReH was performed. In comparison with the other 40 lesions, these lesions had a lower median MRI suspicion score (3 vs 4; $P = 0.003$) and tended to be smaller on ReH (0.49 vs 1.60 mL; $P = 0.08$).

Discussion

Previous studies have explored the associations between PCa volumes determined using MRI and those determined through histolopathological assessment [1-6]. These studies have obtained varying results and are limited in a number of respects, including the use of outdated MRI technology (such as lack of modern multiparametric sequences), imprecise estimates of pathological volume as the reference standard, suboptimal techniques for achieving co-registration of MRI and pathological images, and the use of correlative statistical methods (such as the Pearson correlation coefficient) that do not evaluate true agreement in volume estimations between MRI and pathology. In the present study, we attempted to address these issues by investigating the accuracy of volume estimates from 3T multiparametric MRI using novel co-registration software for comparing the two techniques [9], in addition to the use of software for determining pathological tumour volumes and the Bland–Altman method for assessing true agreement in terms of these volumes.

Through this approach, we obtained different results from those previously obtained in the literature. Overall, MRI substantially underestimated tumour volumes in comparison with histopathology. This underestimation of tumour volume may relate to the findings of Langer et al. [14]. These authors observed that prostate tumours contain regions of sparse tumour comprising mostly benign glands and stroma intermixed with the malignant epithelium. These regions were characterised as inherently invisible on MRI and posing limits on the ability to estimate full tumour volume with MRI. Two subsequent studies confirmed the impact of the histological architecture of prostate tumours in their detection using MRI, with both of these further studies also noting tumours with certain histological characteristics to be predisposed to be undetected [15,16]. One of these studies described the presence of solid tumour growth as a key contributor to tumour detection on MRI that was present in only 57.5% of tumours [15]. It would be anticipated, therefore, that tumour volumes measured

with MRI would underestimate true volume given the presence of such regions within the volume of a tumour. Future studies could perform a more targeted evaluation of those portions of tumour volumes not appreciated on MRI in order to assess the accuracy of this possible explanation.

An unexpected finding was that the degree of underestimation of tumour volumes was more pronounced using the ADC map than using T2WI as well as for tumours with a higher Gleason score or higher MRI suspicion score. Indeed, based on extensive previous literature showing associations between both ADC value and MRI detection with Gleason score [17-20], MRI would have been expected to be more reliable in estimating volume for more aggressive tumours and when recording volume on the ADC map. We note, however, that the previously mentioned studies demonstrating the impact of tumour histological architecture on MRI characteristics focused mainly on the impact on tumour detection rather than on volume estimation [15,16], and it is possible that improved detection of the more aggressive lesions does not directly translate to more accurate volume prediction. In particular, the ADC map was shown to be exquisitely sensitive to the presence of areas of solid tumour growth, with this histological feature more frequently present in higher grade tumours, having a very high odds ratio for lesion detection of 37.6 [15]. We speculate that in more aggressive tumours, these areas of solid tumour formation within the overall tumour margins manifest as clear dark regions on the ADC map, to which the radiologist's attention was directed when estimating lesion volume. This process inherently excluded from volume estimation on MRI any surrounding non-solid lower grade regions, which would be less conspicuous on imaging. Conversely, lower grade lesions, having a smaller component of solid tumour growth, will not have such a conspicuous intra-tumoural abnormality on the ADC map, leading to placement of a broader region of interest in the region of the tumour and resulting in larger volume estimate. This concept could be further explored by direct comparison of MRI findings and pathological characteristics in intra-tumoural sub-regions exhibiting distinct histological features. It is also possible that the sensitivity of T2WI to various benign processes such as inflammation and post-inflammatory atrophy contributed to the apparently larger volumes obtained for T2WI than for ADC.

It is interesting to note that there was a small subset of patients in our cohort in whom the volume predicted on MRI was larger than that obtained from histopathology. These were mainly small tumours with a low MRI suspicion score. Our earlier discussion suggests that these may have included tumours lacking solid tumour growth that confounded reliable volume prediction on MRI; thus, it remains possible that such small low-suspicion lesions can be adequately treated without inclusion of a much larger treatment zone compared with the MRI finding. If validated, this observation could be useful for avoiding unnecessary increases in the duration and complexity of ablation procedures.

The present study has a number of limitations. It was a retrospective study with a relatively small number of patients. In addition, while we provide estimates of the degree of underestimation of tumour volumes using MRI, it is important to note that these tumours are frequently not spherical in shape, such that the extent of underestimation is likely to vary between different directions. Although DCE imaging was viewed when approximating lesion locations, contours were not placed on DCE imaging, given this sequence's lower

spatial resolution and relative lack of technical standardization between centres in terms of acquisition and post-processing. In addition, in our experience, tumour sizes are generally measured on T2WI or DWI in clinical practice [3]. Lastly, variability in estimates of tumour volume between radiologists was not assessed.

In conclusion, estimates of the volume of known prostate tumours using MRI tended to substantially underestimate actual tumour volumes, with wide variability in terms of the extent of this underestimation across individual cases. The underestimation was more pronounced on the ADC map than on T2WI, as well as for tumours with a higher Gleason score and higher MRI suspicion score. These findings have implications for efforts to use MRI to guide risk assessment in candidate selection and choice of treatment of PCa. Future studies may explore the utility of our findings to define a volume surrounding the MRI-based lesion to be covered by targeted therapy.

Acknowledgments

We would like to acknowledge Artem Mikheev for his work on the co-registration process. Funding was received from the Joseph and Diane Steinberg Charitable Trust, an Association Française d'Urologie grant (bourse de l'AFU 2012) and grant 1UL1RR029893 from the National Center for Research Resources, National Institutes of Health.

Abbreviations

PCa	prostate cancer
T2WI	T2-weighted imaging
DWI	diffusion-weighted imaging
ADC	apparent diffusion coefficient
DCE	dynamic contrast-enhanced
3D	three-dimensional
ReH	registered histology

References

1. Jager GJ, Ruijter ET, van de Kaa CA, et al. Local staging of prostate cancer with endorectal MR imaging: correlation with histopathology. AJR Am J Roentgenol. 1996; 166:845–52. [PubMed: 8610561]
2. Villers A, Puech P, Mouton D, Leroy X, Ballereau C, Lemaitre L. Dynamic contrast enhanced, pelvic phased array magnetic resonance imaging of localized prostate cancer for predicting tumor volume: correlation with radical prostatectomy findings. J Urol. 2006; 176(6 Pt 1):2432–7. [PubMed: 17085122]
3. Mazaheri Y, Hricak H, Fine SW, et al. Prostate tumor volume measurement with combined T2-weighted imaging and diffusion-weighted MR: correlation with pathologic tumor volume. Radiology. 2009; 252:449–57. [PubMed: 19703883]
4. Ponchietti R, Di Loro F, Fanfani A, Amorosi A. Estimation of prostate cancer volume by endorectal coil magnetic resonance imaging vs. pathologic volume. Eur Urol. 1999; 35:32–5. [PubMed: 9933792]
5. Coakley FV, Kurhanewicz J, Lu Y, et al. Prostate cancer tumor volume: measurement with endorectal MR and MR spectroscopic imaging. Radiology. 2002; 223:91–7. [PubMed: 11930052]

6. Nakashima J, Tanimoto A, Imai Y, et al. Endorectal MRI for prediction of tumor site, tumor size, and local extension of prostate cancer. Urology. 2004; 64:101–5. [PubMed: 15245944]
7. Turkbey B, Mani H, Aras O, et al. Correlation of magnetic resonance imaging tumor volume with histopathology. J Urol. 2012; 188:1157–63. [PubMed: 22901591]
8. Sosna J, Rofsky NM, Gaston SM, DeWolf WC, Lenkinski RE. Determinations of prostate volume at 3-Tesla using an external phased array coil: comparison to pathologic specimens. Acad Radiol. 2003; 10:846–53. [PubMed: 12945918]
9. Orczyk C, Rusinek H, Rosenkrantz AB, et al. Preliminary experience with a novel method of three-dimensional co-registration of prostate cancer digital histology and in vivo multiparametric MRI. Clin Radiol. 2013; 68:e652–8. [PubMed: 23993149]
10. Hammerer P. pT0 after radical prostatectomy: overtreatment for insignificant prostate cancer? Eur Urol. 2004; 45:35. [PubMed: 14667512]
11. Oto A, Sethi I, Karczmar G, et al. MR imaging-guided focal laser ablation for prostate cancer: phase I trial. Radiology. 2013; 267:932–40. [PubMed: 23440319]
12. Barentsz JO, Richenberg J, Clements R, et al. ESUR prostate MR guidelines 2012. Eur Radiol. 2012; 22:746–57. [PubMed: 22322308]
13. Wysock JS, Rosenkrantz AB, Huang WC, et al. A prospective, blinded comparison of magnetic resonance (MR) imaging-ultrasound fusion and visual estimation in the performance of MR-targeted prostate biopsy: the PROFUS trial. Eur Urol. 2013 in press.
14. Langer DL, van der Kwast TH, Evans AJ, et al. Intermixed normal tissue within prostate cancer: effect on MR imaging measurements of apparent diffusion coefficient and T2-sparse versus dense cancers. Radiology. 2008; 249:900–8. [PubMed: 19011187]
15. Rosenkrantz AB, Mendrinos S, Babb JS, Taneja SS. Prostate cancer foci detected on multiparametric magnetic resonance imaging are histologically distinct from those not detected. J Urol. 2012; 187:2032–8. [PubMed: 22498205]
16. Bratan F, Niaf E, Melodelima C, et al. Influence of imaging and histological factors on prostate cancer detection and localisation on multiparametric MRI: a prospective study. Eur Radiol. 2013; 23:2019–29. [PubMed: 23494494]
17. Verma S, Rajesh A, Morales H, et al. Assessment of aggressiveness of prostate cancer: correlation of apparent diffusion coefficient with histologic grade after radical prostatectomy. AJR Am J Roentgenol. 2011; 196:374–81. [PubMed: 21257890]
18. Woodfield CA, Tung GA, Grand DJ, Pezzullo JA, Machan JT, Renzulli JF 2nd. Diffusion-weighted MRI of peripheral zone prostate cancer: comparison of tumor apparent diffusion coefficient with Gleason score and percentage of tumor on core biopsy. AJR Am J Roentgenol. 2010; 194:W316–322. [PubMed: 20308476]
19. Turkbey B, Shah VP, Pang Y, et al. Is apparent diffusion coefficient associated with clinical risk scores for prostate cancers that are visible on 3-T MR images? Radiology. 2011; 258:488–95. [PubMed: 21177390]
20. Hambrock T, Somford DM, Huisman HJ, et al. Relationship between apparent diffusion coefficients at 3.0-T MR imaging and Gleason grade in peripheral zone prostate cancer. Radiology. 2011; 259:453–61. [PubMed: 21502392]

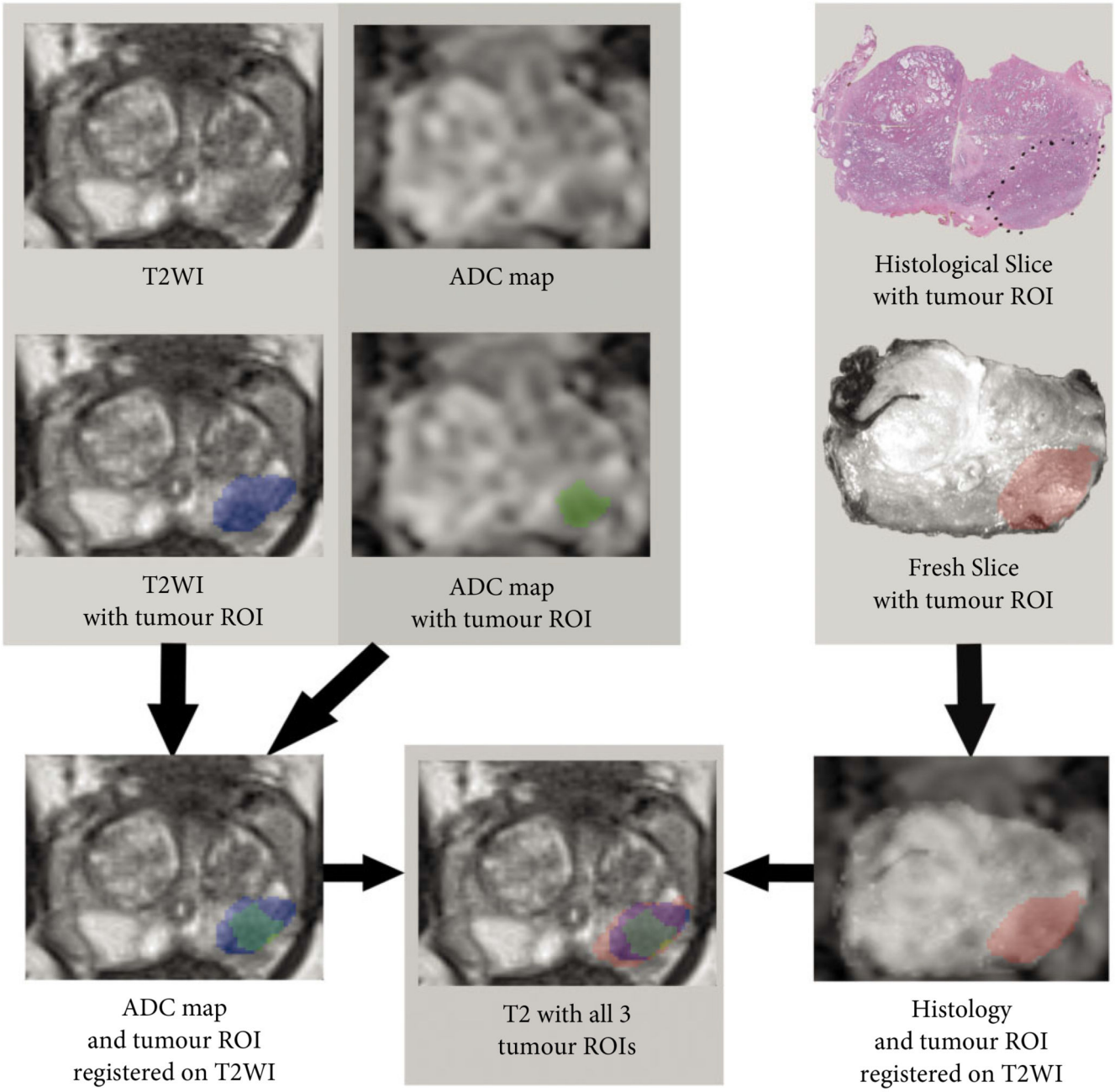

Fig. 1.

Demonstration of co-registration methodology in one case. Tumour is marked in blue, green and red on T2-weighted imaging (T2WI), apparent diffusion coefficient (ADC) and histology, respectively. ROI, region of interest.

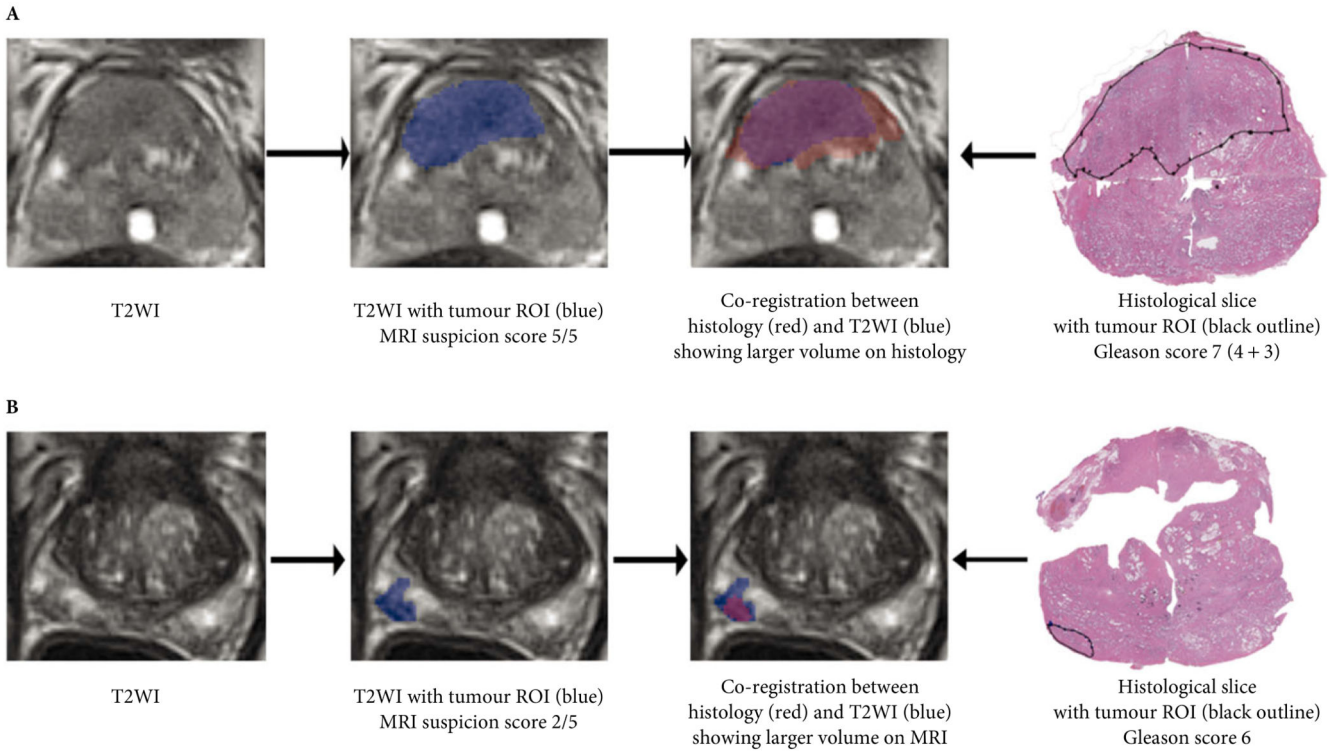

Fig. 2.

Co-registration of tumours between T2-weighted imaging (T2WI) MRI and histology, showing examples of (**A**) larger volume on histology in tumour with Gleason score 7 and MRI suspicion score 5/5, and (**B**) larger volume on MRI in tumour with Gleason score 6 and MRI suspicion score 2/5. ROI, region of interest.

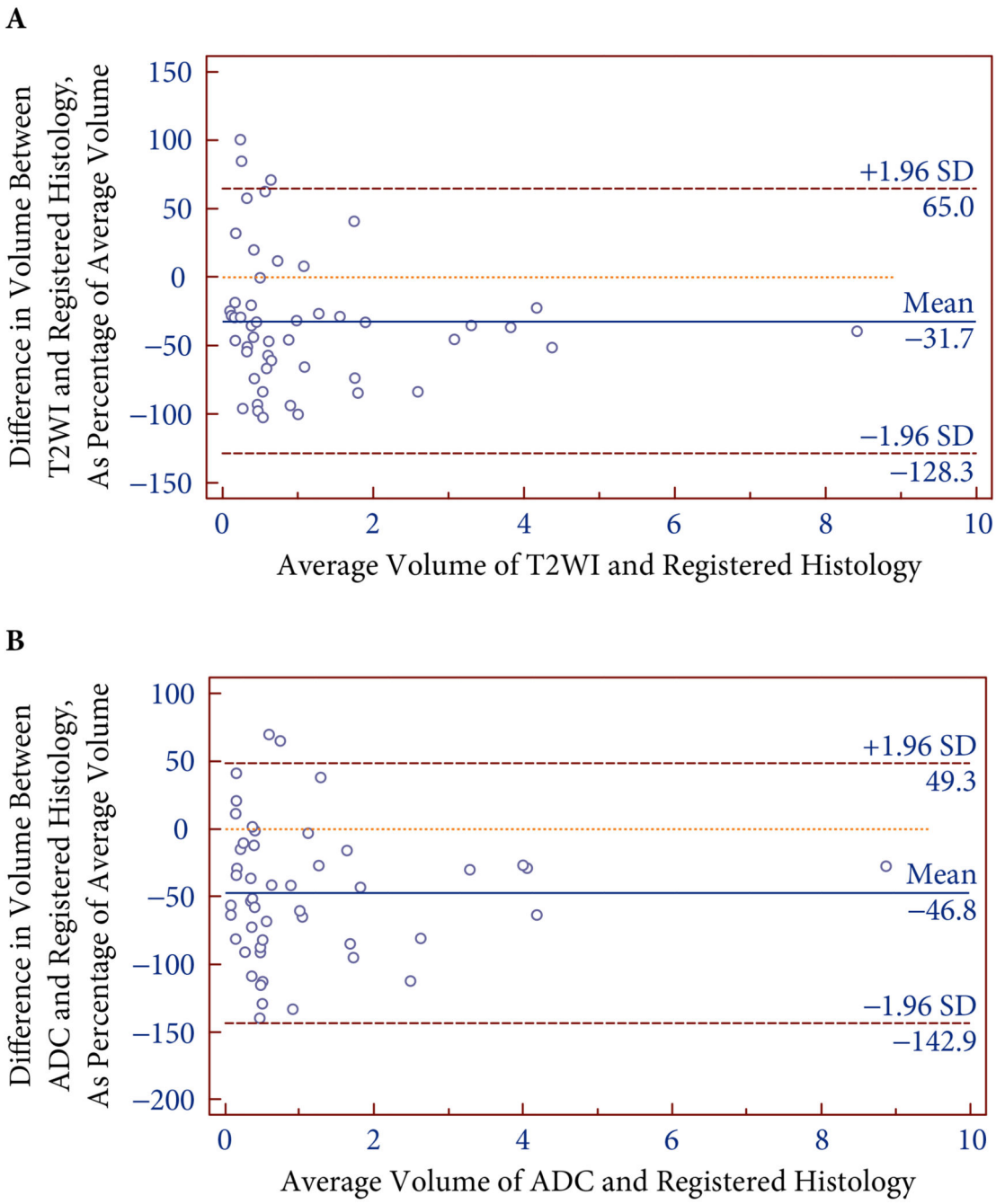

Fig. 3.

Bland-Altman plots comparing volumes of all tumours between registered histology (ReH) and T2-weighted imaging (**A**) and apparent diffusion coefficient (**B**) from preoperative MRI.

Table 1

Characteristics of patients and lesions.

Variable	Mean ± SD	Median	Min	Max
Patients (*n* = 37)				
Age, years	60.3 ± 5.5	62	48	77
PSA, ng/mL	9.5 ± 7.6	5	0.3	98.0
Prostate volume on registered histology, mL	46.6 ± 16.3	42.0	18.0	99.8
Prostate volume on T2-weighted imaging, mL	46.9 ± 16.2	40.1	20.9	106.0
Tumours (*n* = 50)				
Gleason score	–	7	6	9
MRI suspicion score	–	4	2	5
Tumour volume on registered histology, mL	1.38 ± 1.20	0.73	0.11	10.1
Tumour volume on T2-weighted imaging, mL	0.93 ± 0.79	0.45	0.08	6.77
Tumour volume on apparent diffusion coefficient map, mL	0.86 ± 0.78	0.34	0.06	7.69

Table 2

Results of Bland–Altman analyses comparing tumour volumes between MRI sequences and registered histology (ReH).

Sample	T2WI		ADC	
	Mean difference, %	95% limits of agreement, %	Mean difference, %	95% limits of agreement, %
All tumours (*n* = 50)	−32	−128 to +65	−47	−143 to +49
MRI suspicion score 2/3 (*n* = 14)	+2	−107 to +111	−25	−122 to +72
MRI suspicion score 4/5 (*n* = 36)	−45	−97 to +7	−57	−124 to +10
Gleason 6 (11)	−5	−96 to +87	−16	−94 to +63
Gleason ≥7 (*n* = 39)	−39	−104 to +26	−57	−129 to +14
Transition zone (*n* = 10)	−42	−77 to −6	−48	−112 to +16
Peripheral zone (*n* = 40)	−29	−110 to +52	−48	−129 to +33
Histological tumour volume <1 mL (*n* = 31)	−24	−133 to +85	−46	−152 to +60
Histological tumour volume >1 mL (*n* = 19)	−44	−112 to +24	−48	−128 to +31